

Published in final edited form as:

Genesis. 2012 December ; 50(12): 882–891. doi:10.1002/dvg.22342.

Strain-Specific Hyperkyphosis and Megaesophagus in *Add1* null mice

Raymond F. Robledo, Kevin L. Seburn, Anthony Nicholson, and Luanne L. Peters¹

The Jackson Laboratory, Bar Harbor, Maine 04609, USA

Abstract

The three adducin proteins (α , β , γ) share extensive sequence, structural and functional homology. Heterodimers of α - and β -adducin are vital components of the red cell membrane skeleton, which is required to maintain red cell elasticity and structural integrity. In addition to anemia, targeted deletion of the α -adducin gene (*Add1*) reveals unexpected, strain-dependent non-erythroid phenotypes. On an inbred 129 genetic background, *Add1* null mice show abnormal inward curvature of the cervicothoracic spine with complete penetrance. More surprisingly, a subset of 129-*Add1* null mice develop severe megaesophagus, while examination of peripheral nerves reveals a reduced number of axons in 129-*Add1* null mice at four months of age. These unforeseen phenotypes, described here, reveal new functions for adducin and provide new models of mammalian disease.

Keywords

Adducin; Axonal; Gastrointestinal; Spinal; Knockout

Adducin is a component of the spectrin-actin membrane skeleton (Bennett and Baines, 2001; Hughes and Bennett, 1995; Matsuoka et al., 2000). The consequences of an *Add1* loss-of-function mutation were initially described in a C57BL/6J (B6) and 129S1/SvImJ (129) mixed strain of mice (Robledo et al., 2008). Loss of α -adducin resulted in a concomitant loss of both its heterodimer partners, α - and/or γ -adducin, in platelets and red blood cells, which implied that α -adducin is the limiting subunit in tetramer formation in the spectrin-actin junctional complexes. Platelet function remains normal in the absence of adducin. However, loss of adducin in red blood cells results in compensated hemolytic anemia that models human hereditary spherocytosis. Furthermore, approximately fifty percent of the mixed strain null mice developed lethal communicating hydrocephalus, suggesting a role for maintaining cerebrospinal fluid homeostasis. These and additional findings suggest a dynamic role for adducin in assembly, maintenance and regulation of cell membranes (Abdi and Bennett, 2008; Kalfa et al., 2006; Kalfa et al., 2010; Porro et al., 2004; Rabenstein et al., 2005).

In an attempt to limit confounding genetic affects, the *Add1* loss-of-function was bred onto a 129 genetic background to more thoroughly assess the biological roles of α -adducin in mice. Surprisingly, only 10 percent of the offspring from heterozygote matings were *Add1* null at the time of genotyping (P10 to P14), as compared to 16 percent for B6,129 null mice (Table 1) (Robledo et al., 2008). In addition, a number of pups were lost due to unreported deaths

¹Corresponding Author: Luanne L. Peters, PhD The Jackson Laboratory 600 Main Street Bar Harbor, ME 04609. Tel: (207) 288-6391. Fax: (207) 288-6073 luanne.peters@jax.org.

Conflict of Interest Disclosure:

The authors have no conflicts of interest to disclose.

prior to genotyping. The numbers of heterozygous (54.4%) and wild type (33.5%) mice are near expectations when a 15% loss is taken into account. Furthermore, in previous analyses and those to be described here no abnormalities have been seen in heterozygous mice. These observations indicate that null mice are dying perinatally or are being lost *in utero*. Surviving 129-*Add1* null mice are less active and tend to nest or cuddle beneath their normal littermates. Subtle gross abnormalities, including blunter snouts, arching in the back, and splaying of hind legs, begin to appear by five weeks of age (Figure 1). The arching becomes progressively more prominent with age. 129-*Add1* null mice become progressively less active as they age and by 3 weeks of age show markedly decreased body weight compared to normal littermate controls. When suspended by their tail, their limbs tend to splay to the sides and they do not struggle to escape as vigorously as their normal littermates do. They also have stiff and waddle-like gaits. 129-*Add1* null mice are visibly smaller than their littermates at birth and throughout their lifespan (Figure 1). The growth retardation is more severe than that observed in the hybrid B6,129 null mice (Robledo et al., 2008). The longest surviving 129-*Add1* null mouse was a male that reached 11 months, while never obtaining a weight of 20 grams.

129-*Add1* null and wild type littermate mice were scanned by μ CT in order to assess the structural integrity of their spines. 129-*Add1* null mice definitively develop abnormal arching in the cervicothoracic region, as the spine curves inward towards the sternum (Figure 2). On average, one or two dorsal portions of vertebrae appeared to be fused, with the most severe case having all vertebrae of the neck apparently fused (Figure 2b and c). The hyperkyphosis or thoracic lordosis was also associated with scoliosis (Figure 2d). However, evidence of vertebral fusion was not seen in all cases of abnormal spinal curvature. Therefore, fusion was ruled out as the primary etiology. The null mice that generally appear the unhealthiest are the oldest and have the most spinal curvature. This suggests that the inward curving progressively worsens with age. The severity of the abnormal spinal curvature was quantified by modifying the measurement of Cobb's angle (Cobb, 1948). The intersection angle of lines drawn from the third cervical vertebrae and from the eighth thoracic vertebrae was measured (Figure 2e). All 129-*Add1* null mice examined had a significantly larger angle of intersection (Figure 2f).

Tube-like aberrant areas with no density (air) were observed in some of the thoracic cavities of the 129 null mice during the analysis of μ CT scans. Air should have only appeared in the trachea and lungs within the thoracic cavity during μ CT scanning, since the mice were breathing a general anesthetic. The trachea and large airways were ruled out based on the distal anatomical location of the abnormal air-filled structures. Furthermore, dense particle-like structures were co-localizing within these abnormal air-filled areas (Figure 2c). Three-dimensional reconstruction of μ CT scans suggested that the abnormal space was the esophagus. To confirm this conclusion, mice were rescanned following oral gavage of an iodide-based contrasting agent. μ CT and digital reconstructions revealed severely dilated esophagi in some, but not all, 129-*Add1* null mice scanned (Figure 3a thru f). Three null mice were found dead a few days after being μ CT scanned. All three mice were confirmed to have severely dilated esophagi that were packed with undigested food, following necropsy (Figure 3g and h). Routine histology revealed an extremely large esophageal lumen, large quantities of food and in at least one case, evidence of perforation. Enlargement of the esophagi spanned from just below the larynx to the diaphragm. It was also apparent that the stomach did not extend across the diaphragm, thus ruling out hiatal hernia. Furthermore, examination of the digestive tract distal to the esophagus and/or stomach revealed normal morphology and absence of blockage (data not shown). This suggests that the abnormal dense particles, described above, were associated with undigested food. In total, 13 of 29 (45%) 129-*Add1* null mice surviving to adulthood were confirmed to have megaesophagus.

Kyphosis or abnormal sagittal curvature of the spine typically develops when postural muscle tone is lost (Marechal et al., 1996). Taken together, the abnormal spine curvature and megaesophagus in 129-*Add1* null mice suggested the presence of muscle wasting and/or a defect in peripheral innervation, which resulted in lost muscle tone. However, histological analysis of muscle from along affected vertebra, hind legs and esophagi revealed no pathology (Figure 4). Comparison of Cresyl violet, Luxol fast blue and/or Bodian silver stains for the assessment of ganglion was also normal throughout mutant spinal epaxial and hypaxial, diaphragm, longitudinal esophagus and stomach, and cross section femoral vastus, femoris, adductor and gracilis muscle sections (N = 4; data not shown). The sciatic, vagus, femoral sensory, and femoral motor nerves were examined for evidence of peripheral neuropathy as a potential underlying cause of abnormal spinal curvature and/or megaesophagus. Axon numbers were quantified in toluidine stained nerve sections. A significant decrease in axon number of 8.8% was observed in the motor branch of the femoral nerve by four months of age (Figure 5). A greater decrease in axon number of 10% was observed in the sensory branch of the femoral nerve, but it did not reach significance due to greater variability with the relatively small sample size (Figure 5). No differences in axon number within the sciatic nerve were observed (data not shown). The progressive nature of the 129-*Add1* null phenotype could suggest peripheral axonal degeneration, but axonal morphology was normal in all 129-*Add1* null nerves examined.

Add1 null mice are also predisposed to the development of strain-dependent hydrocephalus with the inbred B6 background being the most permissive (Table 2). Indeed, adducin localizes to the basolateral membranes in rat choroid plexus epithelial cells (Marrs et al., 1993). Using alpha-adducin specific antibody (Santa Cruz; 1:25 dilution) and standard techniques, we localized alpha-adducin to the choroid plexus epithelial cell basolateral junctions as well as to those of the ependymal cells lining the 3rd and 4th ventricles in the mouse (not shown). In a group of experiments unrelated to the peripheral nervous system, RNA was obtained from the choroid plexus of six week old B6-*Add1* null, heterozygous and wild type mice and subjected to microarray analysis using the Affymetrix Mouse Gene 1.0 ST Array (data not shown). Of potential interest to the 129-*Add1* phenotype was an observed 2.58 fold decrease in *Nefh* (neurofilament, heavy peptide; $p = 0.001$) expression. Mice deficient in NEFH have been shown to have neurofilament and peripheral axon abnormalities that can progress into neuropathies (Elder et al., 1998; Elder et al., 1999a; Elder et al., 1999b). It is tempting to speculate that NEFH could be similarly down-regulated in other tissue types including the peripheral nervous system in the absence of α -adducin during development, contributing to the observed phenotype in 129-*Add1* null mice. β -adducin has been shown to be required for both synaptic reorganization and assembly at neuromuscular junctions in relation to memory and/or motor coordination (Bednarek and Caroni, 2011; Pielage et al., 2011; Porro et al., 2010; Rabenstein et al., 2005). Therefore, as the adducins function as heterotetramers, it is likely that α -adducin has a similar or complimentary role in maintaining peripheral nerve integrity. Alternative hypotheses for the 129-*Add1* null phenotype include loss of other, currently unidentified binding ligands of the adducins causing structural and/or signaling abnormalities, and loss of adducin regulation of the assembly of spectrin-actin complexes in the cytoskeleton, as has been described in the red cell membrane, platelets and bronchial epithelial cells (Abdi and Bennett, 2008; Barkalow et al., 2003; Hughes and Bennett, 1995).

METHODS

Generation and Maintenance of 129 -*Add1* Null Mice

Generation of mice with a targeted deletion in *Add1* function has been described (Robledo et al., 2008). Since the α -adducin-null mice were generated from the 129P2/HsdOla E14 embryonic stem cell line, resulting chimeric mice were mated to the 129S1/SvImJ inbred

strain to produce the 129-strain of Add1 mice. The mouse colony was sustained by breeding mice heterozygous for the α -adducin-null mutation. All mice were maintained at The Jackson Laboratory in climate- and light cycle-controlled rooms and provided acidified water and 5K52 chow (LabDiet/PMI Nutrition, St. Louis, MO) *ad libitum*. The Jackson Laboratory Animal Care and Use Committee approved all protocols involving mice.

Micro-Computed Tomography (μ CT)

Micro-computed tomography (μ CT) images were obtained using a MicroCAT II scanner combined with BioVet gating hardware and v2.0 software (Siemens Medical Solutions, Malvern PA) that allows imaging to occur during a user-defined segment of the respiratory cycle from anesthetized mice. Anesthesia was induced with 5% isoflurane in oxygen at a rate 0.8 L/min then maintained with 1.5% isoflurane throughout image acquisition. Further definition of esophagi was achieved by injecting 0.25 mL of Isovue (Iopamidol injection; Bracco Diagnostics, Milan, Italy) contrasting agent via oral gavage. Acquired two-dimensional images were reconstructed using the RVA (Siemens Medical Solutions, Malvern PA) real-time reconstruction software. Reconstructed images were further processed using AMIRA v3.10 (Zuse Institute Berlin, Berlin, Germany) software program to create three-dimensional images. A variation of Cobb's angle of abnormal spine curvature (Cobb, 1948) was determined by measuring the angle of intersection of lines drawn from third cervical and eighth thoracic vertebrae, using AMIRA software. A total six Add1-129 null and wild type littermate control mice were analyzed.

Histological Analyses

Skeletal muscle, obtained from along the vertebral column and hind leg, spinal cord and esophagus were fixed in either Bouin or 4% paraformaldehyde fixative by intracardiac perfusion followed by overnight submersion at 4 °C (Sheehan and Hrapchak, 1987). Tissues were paraffin embedded, sectioned at 5 μ M and stained with hematoxylin and eosin, cresyl violet and Luxol fast blue; and Bodian silver stain by standard techniques (Sheehan and Hrapchak, 1987). Peripheral nerve axon number was analyzed as previously described (Burgess et al., 2010; Seburn et al., 2006; Stum et al., 2011). The motor and sensory branches of the femoral nerve and sciatic nerve were dissected and fixed in 0.1 M cacodylate buffered 2% paraformaldehyde and glutaraldehyde overnight at 4 °C. Nerves were embedded in Epon resin, sectioned at 0.5 μ M and stained with Toluidine blue. A minimum of four Add1-129 null and wild type littermate control mice were examined for each staining procedure. Images of tissue sections were acquired using a Leica DMRXE microscope equipped with a Leica DFC 300 FX cooled-CCD color camera and LeicaCam software with a 10 \times , 20 \times , and 40 \times /0.60 objectives (Leica Microsystems, Bannockburn, IL). Myelinated axon number counting was performed using ImageJA (Fiji; <http://pacific.mpi-cbg.de/wiki/index.php/ImageJA>) and the cell counter plugin (cell_counter.jar; <http://rsb.info.nih.gov/plugins/cell.counter.htm>).

RNA Isolation, Processing and Microarray Analysis

Total RNA was extracted from dissected choroid plexi obtained from five α -adducin-wild type, -heterozygous and -null mice on the C57BL/6J background strain at six weeks of age. Choroid plexi were placed directly into TRIzolTM reagent (Invitrogen, Carlsbad, CA) and extracted using the PureLinkTM RNA Micro Kit (Invitrogen, Carlsbad, CA) with DNaseI digestion, as per manufacturer's protocol. cDNA synthesis and Affymetrix Mouse Gene 1.0 ST Array (Affymetrix, Santa Clara, CA) processing was performed as previously described (Vedell et al., 2011). Microarray data generation was compliant with MIAME (<http://www.mged.org/Workgroups/MIAME/miame.html>) standards and has been deposited with Gene Expression Omnibus (GEO: <http://www.ncbi.nlm.nih.gov/geo/>) and assigned the following accession number: GSE37098.

Statistical Analysis

Differences between group data were tested for significance by one-way ANOVA. Tukey honestly significant differences (HSD) test was used to identify significant differences between mean values using JMP v 8.0.1 software (SAS Institute, Cary, NC). *P* values < 0.05 were considered significant.

Average signal intensities for each probe set within arrays were calculated by and exported from Affymetrix's Expression Console (Version 1.1) software using the RMA method which incorporates convolution background correction, sketch-quantile normalization, and summarization based on a multi-array model fit robustly using the median polish algorithm. Four pairwise comparisons were used to statistically resolve gene expression differences between genotype groups using the R/maanova analysis package. Statistical significance levels of the pairwise comparisons were calculated by permutation analysis (1000 permutations) and adjusted for multiple testing using the false discovery rate (FDR), *q*-value method. Differentially expressed genes were declared at an FDR *q*-value threshold of 0.05.

Acknowledgments

Supported by National Institutes of Health grants HL075714 (L.L.P.), The American Heart Association (L.L.P.), and The National Cancer Institute CA34196 (The Jackson Laboratory).

REFERENCES

- Abdi KM, Bennett V. Adducin promotes micrometer-scale organization of beta2-spectrin in lateral membranes of bronchial epithelial cells. *Mol Biol Cell*. 2008; 19:536–545. [PubMed: 18003973]
- Barkalow KL, Italiano JE, Chou DE, Matsuoka Y, Bennett V, Hartwig JH. alpha-Adducin dissociates from F-actin and spectrin during platelet activation. *J Cell Biol*. 2003; 161:557–570. [PubMed: 12743105]
- Bednarek E, Caroni P. beta-Adducin is required for stable assembly of new synapses and improved memory upon environmental enrichment. *Neuron*. 2011; 69:1132–1146. [PubMed: 21435558]
- Bennett V, Baines AJ. Spectrin and ankyrin-based pathways: metazoan inventions for integrating cells into tissues. *Physiol Rev*. 2001; 81:1353–1392. [PubMed: 11427698]
- Burgess RW, Cox GA, Seburn KL. Neuromuscular disease models and analysis. *Methods Mol Biol*. 2010; 602:347–393. [PubMed: 20012408]
- Cobb, JR. Outline for the Study of Scoliosis.. In: Edwards, JW., editor. Instructional Course Lectures, The American Academy of Orthopaedic Surgeons. Ann Arbor, MI: 1948. p. 261-275.
- Elder GA, Friedrich VL Jr. Kang C, Bosco P, Gourov A, Tu PH, Zhang B, Lee VM, Lazzarini RA. Requirement of heavy neurofilament subunit in the development of axons with large calibers. *J Cell Biol*. 1998; 143:195–205. [PubMed: 9763431]
- Elder GA, Friedrich VL Jr. Margita A, Lazzarini RA. Age-related atrophy of motor axons in mice deficient in the mid-sized neurofilament subunit. *J Cell Biol*. 1999a; 146:181–192. [PubMed: 10402469]
- Elder GA, Friedrich VL Jr. Pereira D, Tu PH, Zhang B, Lee VM, Lazzarini RA. Mice with disrupted mid-sized and heavy neurofilament genes lack axonal neurofilaments but have unaltered numbers of axonal microtubules. *J Neurosci Res*. 1999b; 57:23–32. [PubMed: 10397632]
- Hughes CA, Bennett V. Adducin: a physical model with implications for function in assembly of spectrin-actin complexes. *J Biol Chem*. 1995; 270:18990–18996. [PubMed: 7642559]
- Kalfa TA, Pushkaran S, Mohandas N, Hartwig JH, Fowler VM, Johnson JF, Joiner CH, Williams DA, Zheng Y. Rac GTPases regulate the morphology and deformability of the erythrocyte cytoskeleton. *Blood*. 2006; 108:3637–3645. [PubMed: 16882712]
- Kalfa TA, Pushkaran S, Zhang X, Johnson JF, Pan D, Daria D, Geiger H, Cancelas JA, Williams DA, Zheng Y. Rac1 and Rac2 GTPases are necessary for early erythropoietic expansion in the bone marrow but not in the spleen. *Haematologica*. 2010; 95:27–35. [PubMed: 20065081]

- Marechal G, Beckers-Bleukx G, Berquin A, Coulton G. Isoforms of myosin in growing muscles of ky (kyphoscoliotic) mice. *Eur J Biochem.* 1996; 241:916–922. [PubMed: 8944783]
- Marrs JA, Napolitano EW, Murphy-Erdosh C, Mays RW, Reichardt LF, Nelson WJ. Distinguishing roles of the membrane-cytoskeleton and cadherin mediated cell-cell adhesion in generating different Na⁺,K⁺-ATPase distributions in polarized epithelia. *The Journal of cell biology.* 1993; 123:149–164. [PubMed: 8408194]
- Matsuoka Y, Li X, Bennett V. Adducin: structure, function and regulation. *Cell Mol Life Sci.* 2000; 57:884–895. [PubMed: 10950304]
- Pielage J, Bulat V, Zuchero JB, Fetter RD, Davis GW. Hts/Adducin controls synaptic elaboration and elimination. *Neuron.* 2011; 69:1114–1131. [PubMed: 21435557]
- Porro F, Costessi L, Marro ML, Baralle FE, Muro AF. The erythrocyte skeletons of beta-adducin deficient mice have altered levels of tropomyosin, tropomodulin and EcapZ. *FEBS Lett.* 2004; 576:36–40. [PubMed: 15474006]
- Porro F, Rosato-Siri M, Leone E, Costessi L, Iaconcig A, Tongiorgi E, Muro AF. beta-adducin (Add2) KO mice show synaptic plasticity, motor coordination and behavioral deficits accompanied by changes in the expression and phosphorylation levels of the alpha- and gamma-adducin subunits. *Genes Brain Behav.* 2010; 9:84–96. [PubMed: 19900187]
- Rabenstein RL, Addy NA, Caldarone BJ, Asaka Y, Gruenbaum LM, Peters LL, Gilligan DM, Fitzsimonds RM, Picciotto MR. Impaired synaptic plasticity and learning in mice lacking beta-adducin, an actin-regulating protein. *J Neurosci.* 2005; 25:2138–2145. [PubMed: 15728854]
- Robledo RF, Ciciotte SL, Gwynn B, Sahr KE, Gilligan DM, Mohandas N, Peters LL. Targeted deletion of alpha-adducin results in absent beta- and gamma-adducin, compensated hemolytic anemia, and lethal hydrocephalus in mice. *Blood.* 2008; 112:4298–4307. [PubMed: 18723693]
- Seburn KL, Nangle LA, Cox GA, Schimmel P, Burgess RW. An active dominant mutation of glycyl-tRNA synthetase causes neuropathy in a Charcot-Marie-Tooth 2D mouse model. *Neuron.* 2006; 51:715–726. [PubMed: 16982418]
- Sheehan, DC.; Hrapchak, BB. *Theory and practice of Histotechnology.* Second edn. Battelle Press; Columbus, OH: 1987.
- Stum M, McLaughlin HM, Kleinbrink EL, Miers KE, Ackerman SL, Seburn KL, Antonellis A, Burgess RW. An assessment of mechanisms underlying peripheral axonal degeneration caused by aminoacyl-tRNA synthetase mutations. *Mol Cell Neurosci.* 2011; 46:432–443. [PubMed: 21115117]
- Vedell PT, Svenson KL, Churchill GA. Stochastic variation of transcript abundance in C57BL/6J mice. *BMC Genomics.* 2011; 12:167. [PubMed: 21450099]

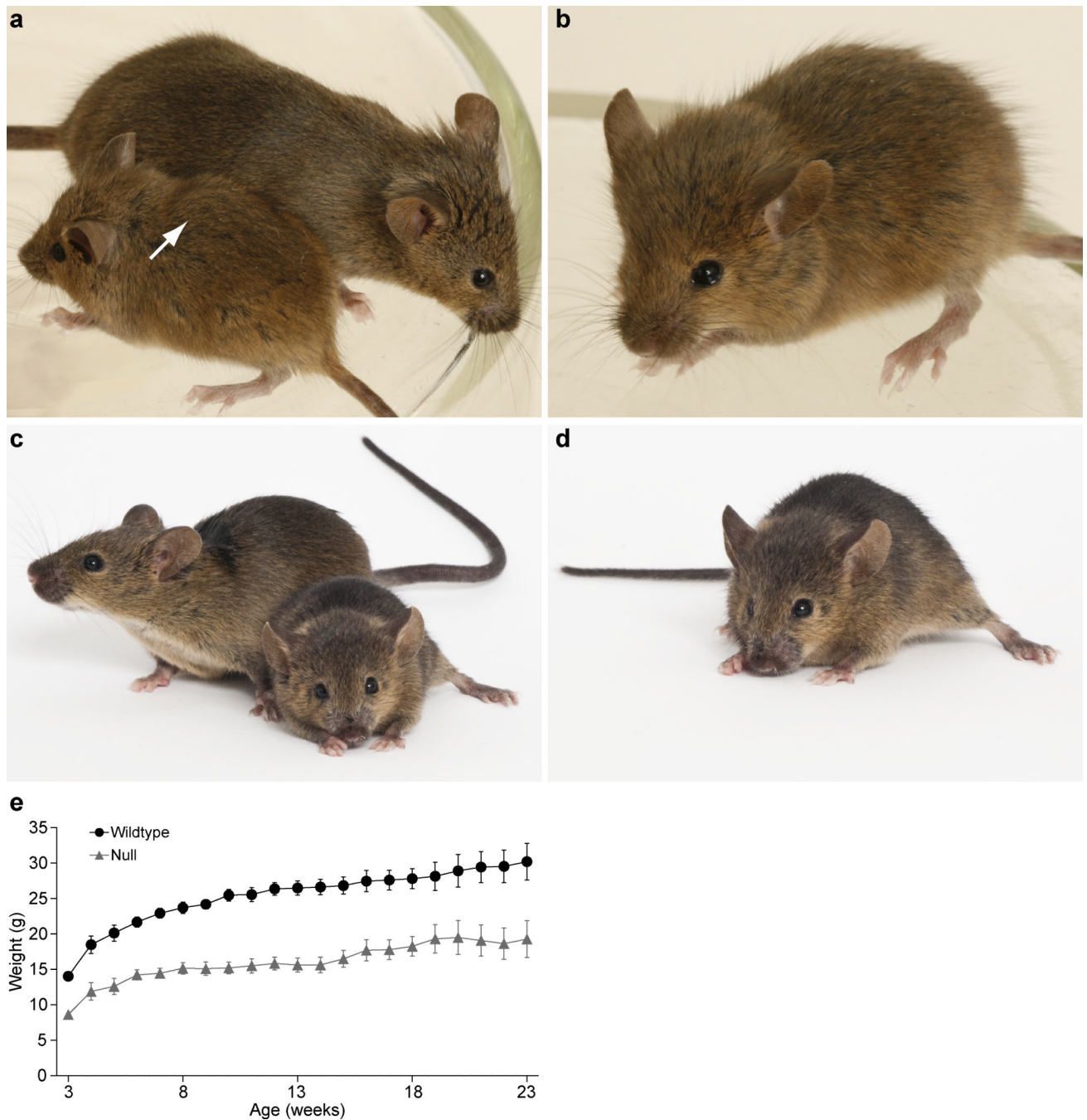


Figure 1. Growth retardation and abnormal physical appearance in α -adducin-129-null mice (a-e) α -adducin-129-null mice are significantly smaller than the wild type and heterozygous littermates from birth throughout their lifespan: wild type and null littermates at (a) five weeks of age and (c) nine weeks of age. Note the abnormal physical appearance characterized by arching of the thoracic region of the back (arrow), splayed hind legs and blunter snout of null mice at 5 (a, b) and 9 (c, d) weeks of age, respectively, as compared to wild type littermates. (e) Growth curve of wild type versus null littermates from three weeks to 23 weeks of age. Note that null mice fail to gain weight at the same pace as their normal

littermates and fall dramatically behind in body weight. Mean weights of all α -adducin-129-null mice at all time points significantly different from wild type ($X \pm SE$; $N=3-5$; $P < 0.05$).

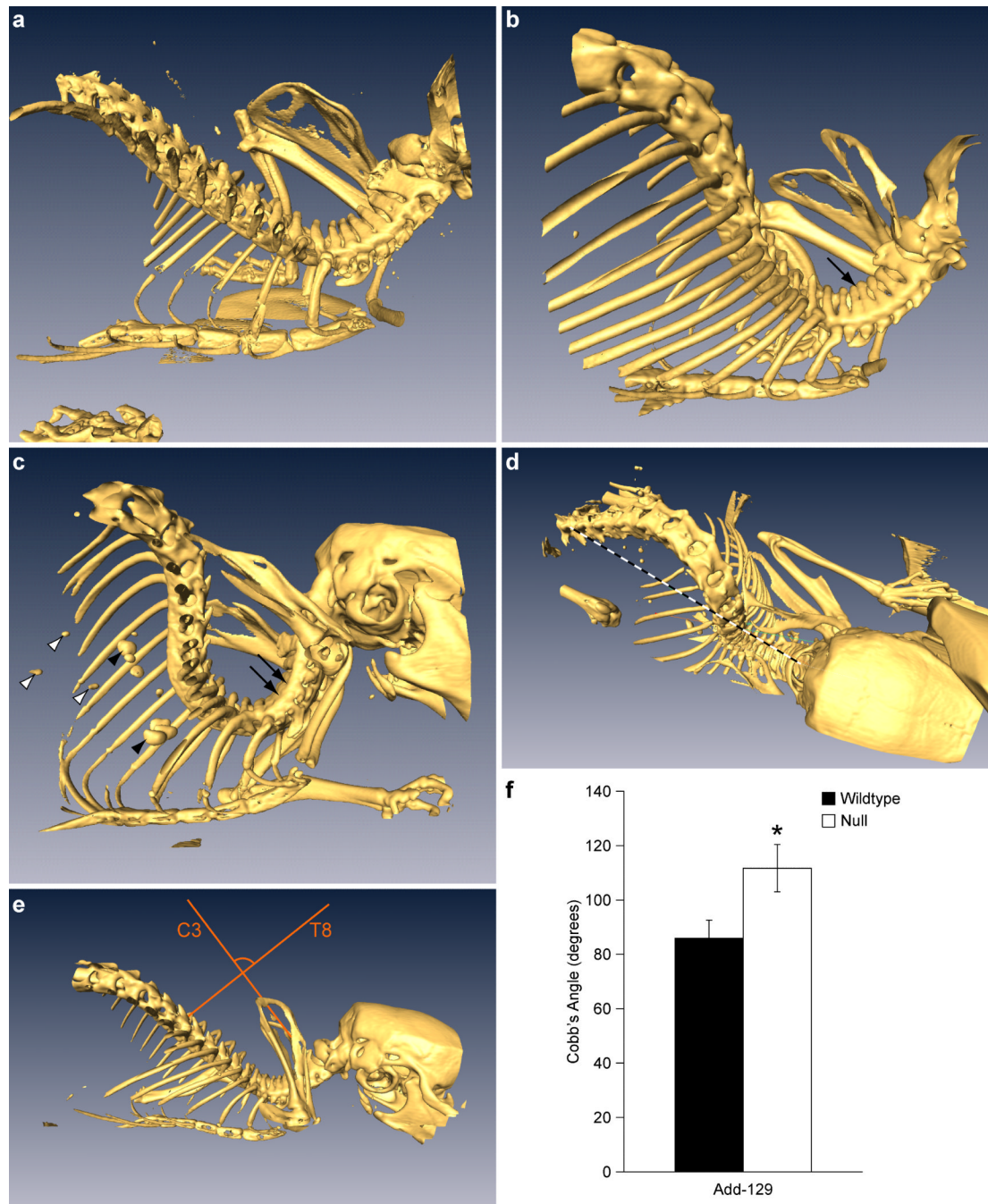


Figure 2. Abnormal inward curving of the cervicothoracic spine of α -adducin-129-null mice
 Three-dimensional μ CT reconstructions of the cervicothoracic spine of wild type (a, e) and α -adducin-129-null (b-d) mice demonstrate abnormal inward curving with fusion of vertebrae (arrows), which becomes progressively more severe in null mice between the ages of 3 (b) and 11 (c) months. Severe cases also present the development of scoliosis (dashed line; d). Also note the presence of abnormal air pockets (arrowheads) and dense particle-like structures (open arrowheads; c). (e, f) Quantification of inward curvature by measuring modified Cobb's angle of intersection from cervical vertebrae three (C3) and thoracic

vertebrae eight (T8) results in α -adducin-129-null mice having a significantly (*) higher angle of intersection as compared to wild type littermates ($X \pm SE$; N=6).

\$watermark-text

\$watermark-text

\$watermark-text

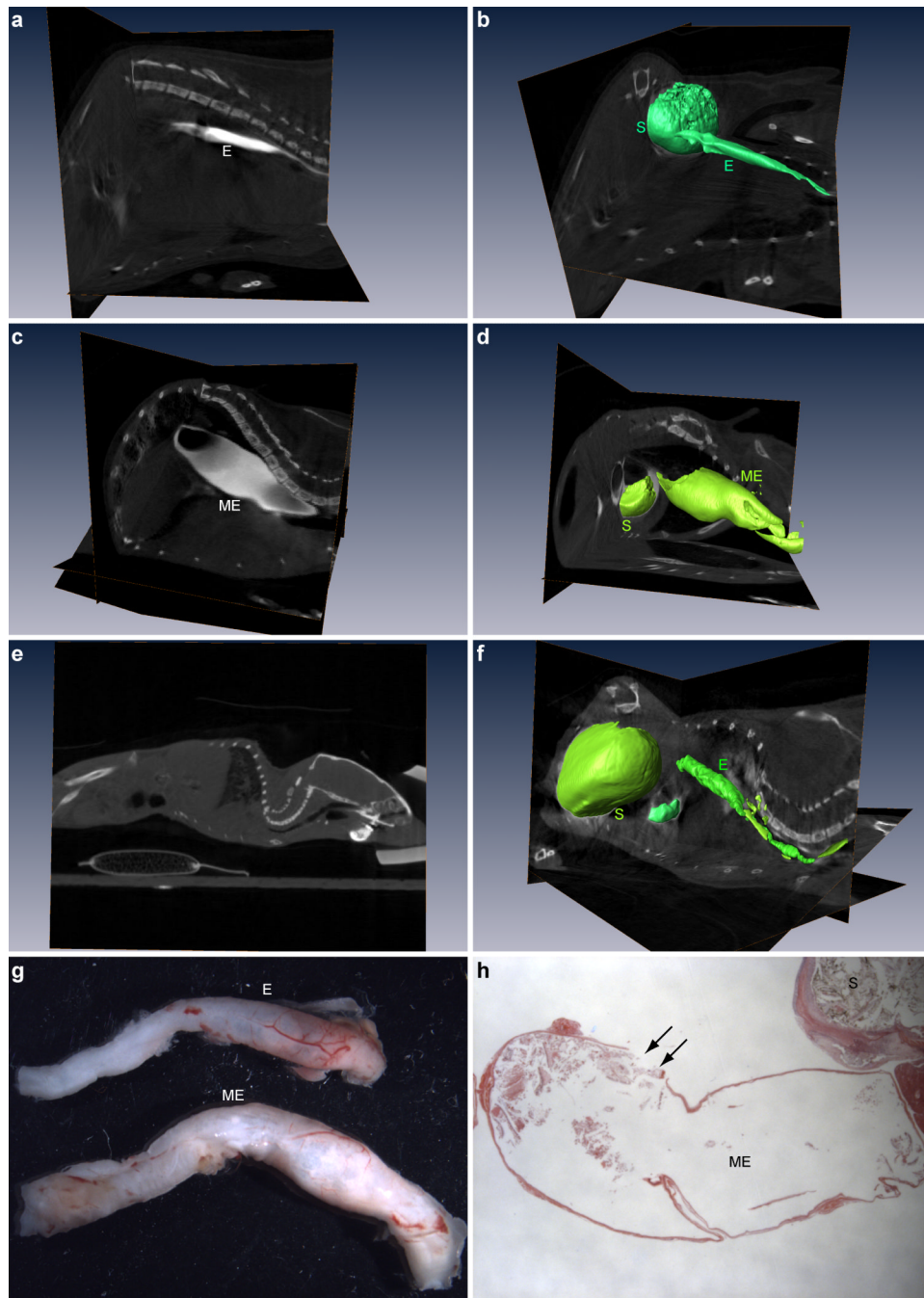


Figure 3. α -adducin-129-null mice develop megaesophagus with variable penetrance (a-f) μ CT scans with (a-d, f) or without (e) Isovue contrasting agent and representative three-dimensional reconstructions of wild type (a, b) and α -adducin-129-null (c-f) esophagi reveal the development of megaesophagus in null mice (c, d) with variable penetrance (d vs. f). Nevertheless, null mice failing to develop megaesophagus present with abnormal spine curvature (e, f). (g) Side by side comparison of fixed en bloc esophagi dissected from six month old littermates (lower = null). (h) Postmortem hematoxylin and eosin stained megaesophagus from 11 month old 16.2 g α -adducin-129-null mouse (original

magnification of 20X). Note thinning of esophageal walls and apparent perforation (arrows) from excessive distension. Esophagus (E); Megaesophagus (ME); Stomach (S).

\$watermark-text

\$watermark-text

\$watermark-text

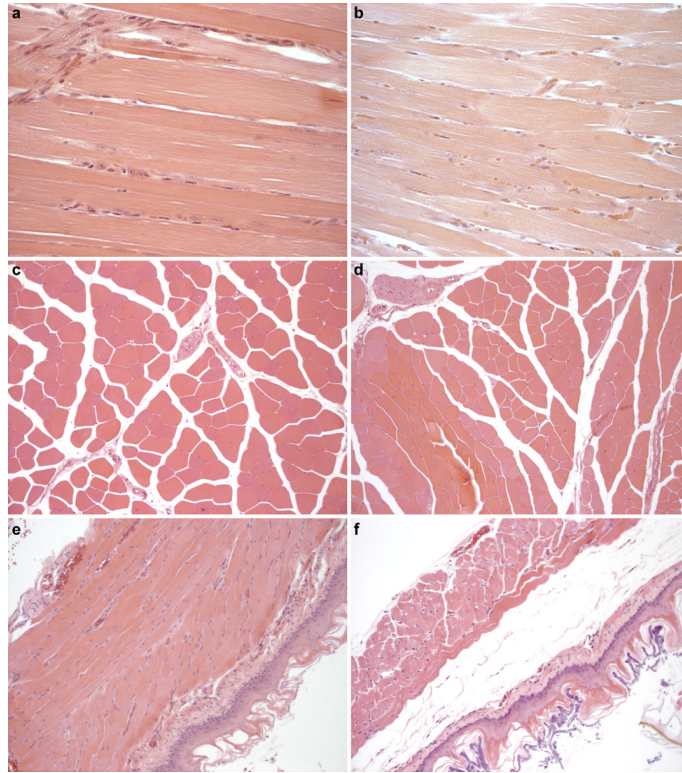


Figure 4. Normal muscular and esophageal morphology in α -adducin-129-null mice
Hematoxylin and eosin stained sections fail to demonstrate muscular dystrophy or atrophy along the spine (**a, b**), hind leg (**c, d**) or esophagus (**e, f**) in α -adducin-129-null mice (**b, d, f**) relative to wild type littermates (**a, c, e**). Images were captured with original magnifications of 200X.

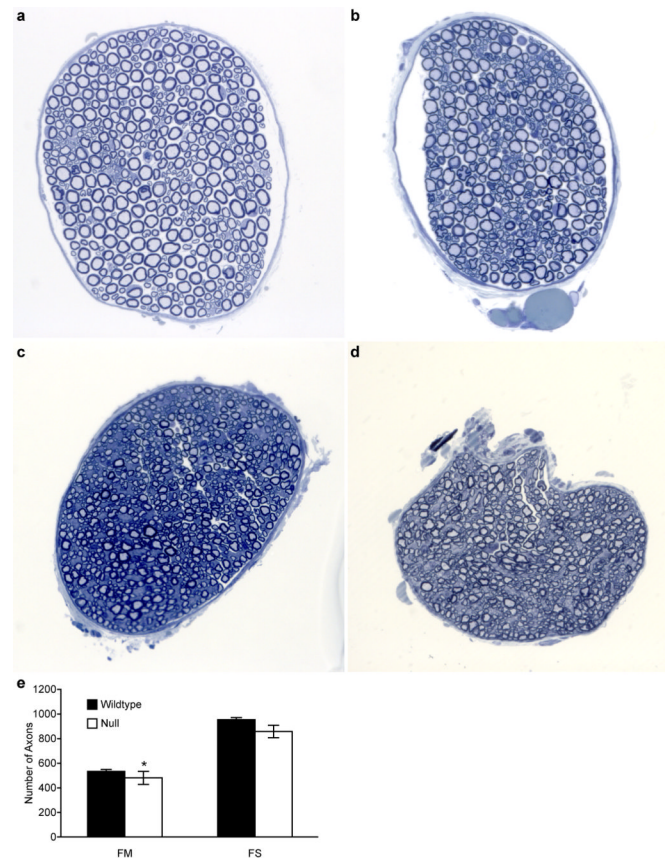


Figure 5. α -adducin-129-null mice develop a reduced number of femoral nerve axons

Toluidine blue stained cross section through the motor (a, b) and sensory (c, d) branches of the femoral nerves from wild type (a, c) and α -adducin-129-null (b, d) mice at four months of age. By and large, axon morphology of null nerves is normal relative to wild type littermates. Quantification of the number of axons in nerve branch reveals a significant (*) loss in the motor branch of null mice (e; $X \pm SE$; $N=4$ for both groups; $P < 0.05$). There is a greater loss in sensory branch axons that did not reach a level of significance due to increased variability.

\$watermark-text

\$watermark-text

\$watermark-text

Table 1

Genotype Distribution of 129-*Add1* Targeted Mice

Litters	Total Mice	<i>Add1</i> ^{+/+}	<i>Add1</i> ^{+/-}	<i>Add1</i> ^{-/-}	Missing
59	283	97	157	29 ^{*#}	7
Percentage		33.45	54.14	10.00	2.41

^{*} 29 of 29 (100%) *Add1*^{-/-} developed hyperkyphosis
[#] 14 of 29 (48.28%) *Add1*^{-/-} developed megaesophagus or megastomach

Table 2Frequency of *Add1*-null Phenotypes by Background Strain.

Strain	Hydrocephalus	Kyphosis	Megaesophagus	Megastomach
129S1/SvImJ (129)	1/29	29/29	13/29	1/29
C57BL/6J (B6)	57/71	0/71	0/71	0/71
B6;129	50/98 *	0/98	0/98	0/98

*
(Robledo et al., 2008)